INSTITUTE OF PHYSICS PUBLISHING PHYSICS IN MEDICINE AND BIOLOGY

Phys. Med. Biol. **47** (2002) 3387–3405 PII: S0031-9155(02)36005-6

Quantitative fluorescence lifetime spectroscopy in turbid media: comparison of theoretical, experimental and computational methods

Karthik Vishwanath[1], **Brian Pogue**[2] **and Mary-Ann Mycek**[1]

[1] Department of Physics and Astronomy, Dartmouth College, Hanover, NH 03755, USA
[2] Thayer School of Engineering, Dartmouth College, Hanover, NH 03755, USA

E-mail: mycek@dartmouth.edu

Received 19 April 2002
Published 5 September 2002
Online at stacks.iop.org/PMB/47/3387

Abstract

A Monte Carlo model developed to simulate time-resolved fluorescence propagation in a semi-infinite turbid medium was validated against previously reported theoretical and computational results. Model simulations were compared to experimental measurements of fluorescence spectra and lifetimes on tissue-simulating phantoms for single and dual fibre-optic probe geometries. Experiments and simulations using a single probe revealed that scattering-induced artefacts appeared in fluorescence emission spectra, while fluorescence lifetimes were unchanged. Although fluorescence lifetime measurements are generally more robust to scattering artefacts than are measurements of fluorescence spectra, in the dual-probe geometry scattering-induced changes in apparent lifetime were predicted both from diffusion theory and via Monte Carlo simulation, as well as measured experimentally. In all cases, the recovered apparent lifetime increased with increasing scattering and increasing source–detector separation. Diffusion theory consistently underestimated the magnitude of these increases in apparent lifetime (predicting a maximum increase of $\sim$15%), while Monte Carlo simulations and experiment were closely matched (showing increases as large as 30%). These results indicate that quantitative simulations of time-resolved fluorescence propagation in turbid media will be important for accurate recovery of fluorophore lifetimes in biological spectroscopy and imaging applications.

1. Introduction

Studies of photon propagation in turbid, inhomogeneous media (such as biological tissues) have increased in recent years in response to expanding interest in applications of light for biomedical diagnostic and therapeutic use (Welch and van-Gemert 1995, Cheong *et al*

1990, Das *et al* 1997, Rudolph and Kempe 1997, Wagnières *et al* 1998). Areas of interest include biological fluorescence spectroscopy and imaging using both endogenous and exogenous fluorophores (Richards-Kortum and Sevick-Muraca 1996). Endogenous biological fluorophores include structural proteins (e.g., collagen, elastin), metabolic co-factors (e.g., flavins, reduced pyridine nucleotides) and amino acids (e.g., tryptophan, tyrosine). Fluorescence methods can provide information about the physiological state (biochemical and morphological) of cells and tissues (Richards-Kortum 1995, Zeng *et al* 1998, Schomacker *et al* 1992, Dhingra *et al* 1996), and have been applied in the form of both steady-state (spectral) and time-resolved (lifetime) measurements for basic biological studies and to aid in clinical diagnostics. Steady-state fluorescence has been employed to analyse fluorescent reporters of metabolic processes (Fantini *et al* 1994, Frisoli *et al* 1993, Konig *et al* 1992) and to monitor drug dosage and treatment effects in photodynamic therapy (Wagnières *et al* 1998, Pogue *et al* 2001, Lee *et al* 2001). Although spectrally resolved fluorescence measurements are relatively simple to implement clinically, they are inherently intensity dependent. Thus, wavelength-dependent variations in collected intensity due to sources of optical loss (both from an experimental set-up and from the effect of local tissue absorption and scattering properties) can affect the lineshape of fluorescence spectra in complex and unpredictable ways (Lakowicz 1999). Since a spectrum is obtained by integrating emitted fluorescence photons over time, the resulting data ignore the dynamics of the fluorescence emission process, thereby losing an additional dimension of temporal (lifetime) information. Typical fluorescence spectra from biological molecules have broad, featureless emission bands due to molecular vibrations and non-radiant relaxation and their lineshapes may appear relatively insensitive to local biochemistry.

Some of these limitations may be addressed by fluorescence lifetime methods, which measure the fluorophore's average excited state lifetime, and thus provide information complementary to that obtained from steady-state spectral measurements. Fluorescence lifetimes may be measured by using time- or frequency-domain methods (Lakowicz 1999). Frequency-domain approaches to determine fluorescence lifetimes (Hutchinson *et al* 1996, Paithankar *et al* 1997, 1999, Sevick-Muraca *et al* 1998) use amplitude and frequency modulated excitation sources and detect phase shifts and amplitude variations in the remitted fluorescence. The time-domain approach uses pulsed excitation sources and measurements that capture the transient decay of fluorescence intensity in time. This decay profile reflects the relative concentrations and the excited state lifetimes of the constituent fluorophores (Hutchinson *et al* 1995), and can be used to determine tissue optical properties (Das *et al* 1997). Fluorophore lifetimes, which depend on both radiative and non-radiative decay mechanisms, are known to be very sensitive to the local biochemical environment and to vary with pH, molecular binding and oxygenation, all of which may differ between diseased and normal tissues (Lakowicz 1999, Vaupel *et al* 1989). Because intrinsic fluorophore lifetimes are invariant to changes in excitation intensity or sources of optical losses, time-resolved measurements are considered to be intensity independent. Studies have employed lifetime spectroscopy as a diagnostic tool for several medical applications including early cancer detection and staging atherosclerotic plaque (Pfeifer *et al* 1995, Alfano *et al* 1998, Beauvoit and Chance 1998, Glanzmann 1998, Mycek *et al* 1998, 2000, Pradhan *et al* 1992).

Quantitative fluorescence spectroscopy for biomedical applications is hampered by difficulties in interpreting fluorescence signals obtained from fluorophores buried in highly scattering and absorbing inhomogeneous media, such as biological tissues. Analytical treatment of light propagation in tissue is possible by considering light to be composed of neutral particles, and applying the radiative transport equation to describe photon propagation in such turbid media (Chandrasekhar 1960). A common simplification to this approach

has been to use the diffusion approximation to the radiative transport equation, which yields analytical solutions for the light energy distribution, both spatially and temporally, when applied to simple geometries (Wu *et al* 1993, Star *et al* 1988, Patterson and Pogue 1994). While several researchers have shown that steady-state fluorescence signals originating from scattering media can be predicted given the fluorophore concentration and the optical interaction parameters intrinsic to the medium (Wu *et al* 1993), analytical approaches to predict time-resolved fluorescence are limited (Hattery *et al* 2001, Sadoqi *et al* 2001).

Ultimately, the mathematical intractability and the assumptions inherent in such theoretical approaches are significant, and have limited the utility of the diffusion theory approximation in tissues that have complex geometries or multiple constituents. Alternative stochastic approaches can be used to model photon transport in turbid media. Monte Carlo modelling was first applied to study light dosimetry in tissues in 1983 (Wilson and Adam 1983) and has been shown to provide the most accurate results in comparison with the experiment (Wang *et al* 1997, 1995, Zeng *et al* 1997, Flock *et al* 1989, Welch *et al* 1997). While diffusion theory solutions have been developed to the point of simulating fluorophore lifetimes in bulk tissues, comparatively little work has been done to model tissue fluorophore lifetimes using the stochastic approach (Yaroslavsky *et al* 1997). Development of accurate stochastic simulations of fluorescence propagation in tissue, including the recovery of fluorophore lifetimes, would aid in quantitatively understanding the origin of these complex biological signals.

In the study reported here, we present a Monte Carlo model that is used to simulate time-resolved fluorescence from a homogeneous semi-infinite turbid medium with a fixed concentration of a single fluorophore species using fibre-optic probes for illumination and detection. The simulations are first tested for accuracy by comparison to previously reported models and to theoretical diffusion theory expressions for both steady-state and time-resolved reflectance expressions and to theoretical diffusion theory expressions for time-resolved fluorescence. The simulation is then used to predict the variations in apparent lifetime for a single (known) fluorophore concentration present in the medium, by varying two parameters: (a) the scattering properties of the medium, (b) the source–detector separation. The results of the simulation are then compared to experimental steady-state and time-resolved fluorescence measurements on tissue phantom media. Results showing the apparent changes in the recovered fluorophore lifetime with changes in optical scattering and source–detector geometry are quantified and discussed.

2. Theory

2.1. Monte Carlo model

Monte Carlo computational methods have been applied to a variety of problems in neutron and photon random-walk type problems (Cashwell and Everett 1959, Lux and Koblinger 1991). The rationale for using Monte Carlo methods to study problems of light distribution in tissue has been described (Wang *et al* 1995, Wilson and Adam 1983). An important advantage of using a Monte Carlo simulation is the ease with which source distributions and collection geometries can be modelled in the simulation, making it possible to rapidly examine multiple experimental designs via model predictions (Testorf *et al* 1999, Song *et al* 1999, Prahl 1988, Flock *et al* 1989, Pogue and Burke 1998). For the studies reported here, we developed a Monte Carlo model that can simulate arbitrary source–detector fibre geometries, fibre optical properties and record time-resolved information for both excitation and fluorescent light (emanating from a fluorophore inside a semi-infinite medium), as shown schematically in figure 1.

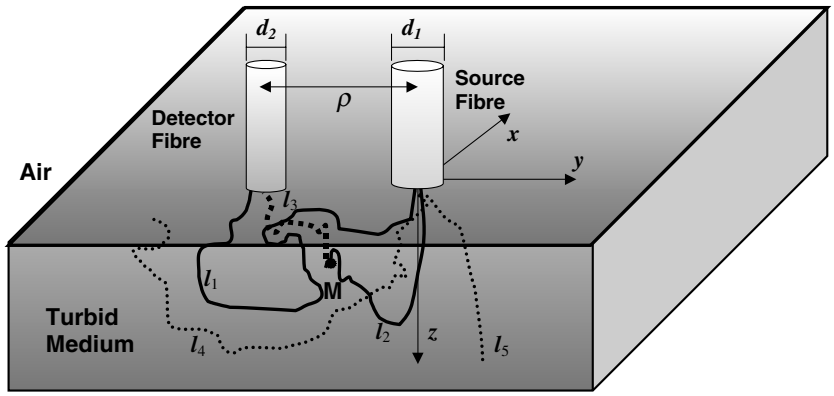

Figure 1. Schematic of the simulation and experiment. The semi-infinite layer has homogenous optical coefficients and is infinite in extent along the xy plane. The direction of incident light is normal to the surface along the z-axis. Path l_1 indicates an excitation photon reaching the detector. Path l_2 shows an excitation photon generating a fluorescence photon at M, which travels the dotted path, l_3, before reaching the detector. Paths l_4 and l_5 show excitation photons (dashed paths) that are not detected. Here, d_1 and d_2 are the source and detector fibre diameters, respectively, while ρ indicates the centre-to-centre separation between the fibres.

In the simulation, photons are launched individually into a turbid medium via an optical fibre of specified diameter and numerical aperture. The fibre optic is assumed to be resting on the surface of the turbid medium and hence there are no mismatched boundaries in this model. The average interaction path length, l, between the photon and the medium is given by $l = 1/\mu_t$, where μ_t is the total attenuation coefficient (also called the extinction coefficient) and is given as the sum of the absorption (μ_a) and scattering (μ_s) coefficients. The simulation functions by making each photon travel a step of length, s_i, in the tissue. As described previously (Wang *et al* 1995), this variable step size is sampled by using a random number, ξ, uniformly distributed between 0 and 1 such that the size of the step is given by

$$s_i = -\frac{\ln(\xi)}{\mu_t}. \tag{1}$$

Equation (1) creates a step size based on a random number, ξ, generated by the computer, and on averaging s_i for a large number of steps, the mean step size is l if the random number generator has a uniform distribution (Wang *et al* 1995). In order to account for photon absorption by the medium, each photon begins its flight with a weight of unity, and, after each step s_i, the weight of the photon is attenuated according to Beer's law (Welch and van-Gemert 1995). Thus, after the ith step, the photon weight is given as $w_i = w_{i-1}\exp(-\mu_a s_i)$, where w_{i-1} is the photon weight before the ith step (Pogue and Burke 1998). This method for photon weight attenuation using Beer's law varies slightly from another method using an approximation to Beer's law (where $w_i = w_{i-1}(1 - \mu_a/\mu_s)$) as described in Wang *et al* (1995). When the media's absorption coefficient is comparable to its scattering coefficient, the method used here, based on the exact application of Beer's law, provides a more accurate solution, albeit being less efficient to model computationally.

The photon's path in the semi-infinite medium ends when it crosses the tissue–air interface or when its weight falls below a threshold minimum value (set to 1×10^{-5} in this study). At the end of its travel in the tissue, the total path length, L, of the photon contains information about the time the photon has spent in the tissue (Jacques 1989). This temporal information maybe binned using a binning value, Δt, which determines the temporal resolution of the

simulation. Thus, the time, t, spent by the photon inside the medium is given by $t = L/nc$, where c is the velocity of light in vacuum and n is the refractive index of the medium. The simulation stores this temporal information as a linear array, where the index j of the array is calculated by

$$j = \mathrm{INT}\left(\frac{t}{\Delta t}\right) \tag{2}$$

where INT is a function that returns the largest integer less than its argument.

After each scattering step, the new direction of the photon's travel is recalculated as governed by the scattering phase function for the tissue. The model developed for the studies reported here uses the Henyey–Greenstein function to sample the scattering angles between photon–tissue interactions. This phase scattering probability density function was originally proposed (Henyey and Greenstein 1941) for galactic light scattering, and approximates the Mie scattering of light waves by particles whose sizes are comparable to the wavelength of light. This phase function has been shown to provide a reasonable approximation to the scattering function in tissue (Wang *et al* 1997), while research continues to find improved phase functions to provide more accurate simulations of photon propagation over short distances (Mourant *et al* 1996).

Each photon begins its flight inside the tissue as an excitation photon. To simulate fluorescence emission, before each scattering event of an excitation photon, another random number (between 0 and 1), ξ', is generated and compared to a fluorophore absorption threshold value, κ, where $\kappa = [1 - \exp(\mu_{af} s_i)]$, and μ_{af} is the coefficient of fluorophore absorption (Pogue and Burke 1998). If ξ' is less than κ, the excitation photon is tagged a fluorescence photon, its new direction of travel is determined by an isotropic scattering event and its weight, w_i, is multiplied by the fluorescence quantum yield, Φ_{QY}. This newly created fluorescence photon then continues to propagate from that point, as governed by the scattering, absorption and anisotropy coefficients of the medium at the fluorescence emission wavelength. This method for simulating fluorescence can be understood as an interpretation of Beer's law, where κ represents the probability that an excitation photon is absorbed by a fluorophore in the medium over a step of size s_i. The probability distribution of the random number, ξ', is known to be unity. Hence, every sampling of ξ' that is less than κ results in both the absorption of an excitation photon by the fluorophore and the weighted isotropic remission of an emitted fluorescence photon. We note that the coefficients of absorption and scattering for the fluorescence and excitation photons may be different and are therefore introduced separately in the model.

Incorporating fluorophore lifetimes into the Monte Carlo algorithm requires one further step in the simulation. By definition, the fluorophore lifetime, τ_0, is the average amount of time electrons spend in the excited state (Lakowicz 1999). Electrons that decay to the ground state non-radiatively are accounted for by the fluorescence quantum yield, Φ_{QY}. Electrons that decay radiatively emit fluorescence photons that the simulation delays in time by a variable factor t_d, before accumulating them in the linear temporal array described above, where t_d is given by

$$t_d = -\tau_0 \ln(\xi''). \tag{3}$$

Here ξ'' is a random variable (between 0 and 1) generated by the computer and the logarithm term arises from mapping the probability distribution governing the fluorophore lifetime to the probability distribution of the computer's random number generator using a Monte Carlo method (Wang *et al* 1995).

2.2. Diffusion theory

The radiative transport equation (Chandrasekhar 1960) is a well-known analytical model describing the photon radiance at any point within a turbid medium. The differentio-integral form of the transport equation prevents finding analytical solutions for problems of practical interest in laser medicine, which may require the incorporation of multiple sources and detectors or the description of layered, inhomogeneous media. A useful approximation to the transport equation, valid when the medium's absorption is small in comparison to its scattering and when points of observation are far from sources and boundaries, effectively describes diffusive photon propagation in a turbid medium (Welch and van-Gemert 1995). This diffusion equation can be solved for the light distribution either temporally or spatially, given specific boundary conditions (Patterson *et al* 1989, Welch and van-Gemert 1995, Haskell 1994, Kienle and Patterson 1997). Presented below are results from the application of diffusion theory to homogeneous turbid media, which are used to validate the performance of the simulation.

The expression for the normalized steady-state reflectance as calculated for a semi-infinite turbid medium using an extrapolated boundary condition is given by the expression (Farrell *et al* 1992)

$$R(\rho) = \frac{1}{4\pi}\left(\frac{1}{\mu_t'}\left(\mu_{\text{eff}} + \frac{1}{r_1(\rho)}\right)\frac{\exp(-\mu_{\text{eff}} r_1(\rho))}{r_1(\rho)} + \left(\frac{1}{\mu_t'} + 4D\right)\left(\mu_{\text{eff}} + \frac{1}{r_2(\rho)}\right)\frac{\exp(-\mu_{\text{eff}} r_2(\rho))}{r_2(\rho)}\right). \tag{4}$$

Here ρ is the distance from the source to the detector, $R(\rho)$ is the collected reflectance, and μ_s, μ_a and g are the scattering, absorption and anisotropy coefficients, respectively, for the given wavelength and medium under investigation. The other terms in (4) are given as

$$r_1(\rho) = \sqrt{\rho^2 + \frac{1}{\mu_t'^2}} \tag{5}$$

$$r_2(\rho) = \sqrt{\rho^2 + \left(\frac{1}{\mu_t'} + 4D\right)^2} \tag{6}$$

$$\mu_t' = (1-g)\mu_s + \mu_a \tag{7}$$

$$\mu_{\text{eff}} = \sqrt{3\mu_a\mu_t'} \tag{8}$$

$$D = (3\mu_t')^{-1}. \tag{9}$$

The time-resolved expression for the normalized reflectance from a semi-infinite surface, with a delta function source, has also derived (Flock *et al* 1989):

$$R(\rho, t) = t^{-\frac{5}{2}} \exp\left(-\frac{\rho^2 + \left(\frac{1}{\mu_t'}\right)^2}{4Dct}\right)\exp(-\beta_x t) \tag{10}$$

where c is the velocity of light in the medium, $\beta_x = c(\mu_{af} + \mu_a)$, and μ_{af} is the coefficient of absorption of any fluorophore present in the medium. We note that the subscript x indicates that the absorption coefficients are evaluated at the excitation wavelength.

A later study (Patterson and Pogue 1994) extended equation (10) to describe the time-resolved propagation of fluorescent light from a semi-infinite turbid medium containing a

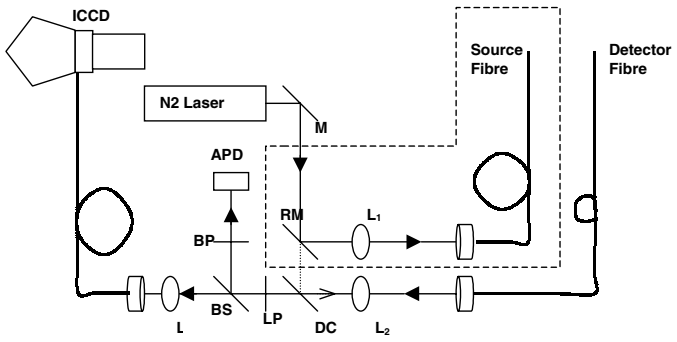

Figure 2. Schematic of the instrumentation: ICCD—intensified charge couple device; APD—avalanche photodiode; M—mirror; RM—retractable mirror; DC—dichroic mirror; L_1/L_2—lens; LP—long pass filter; BS—beam splitter; BP—band pass filter. The dashed box shows how inserting the mirror RM changes the set-up from a single-fibre configuration to a dual-fibre configuration.

fluorophore when excited by a delta-function source. Neglecting the lifetime component, the normalized fluorescence can be expressed as

$$F(\rho,t) = t^{-\frac{5}{2}} \exp\left(-\frac{\rho^2 + \left(\frac{1}{m\mu_t'}\right)^2}{4Dct}\right)[\exp(-\beta_m t) - \exp(-\beta_x t)] \tag{11}$$

where $\beta_m = c(\mu_{af} + \mu_a)$ and the subscript m indicates that the tissue coefficients correspond to the emission wavelength. In a medium containing n fluorophores, with the ith fluorophore lifetime being given by τ_i, equation (11) may be convolved as

$$F_\tau(\rho,t) = F(\rho,t) \otimes \sum_{i=1}^{n} \frac{1}{\tau_i} \exp\left(-\frac{t}{\tau_i}\right) \tag{12}$$

to yield the correct expression for time-resolved fluorescent light propagation. The theoretical results presented here will be used below to validate our simulation's performance in studies of steady-state and time-resolved reflectance, as well as time-resolved fluorescence.

3. Experiment

Experimental validation of the computational model developed above involved preparing tissue phantoms with well-defined absorption and scattering properties. Measurements were then made on these phantoms using a modified fluorescence lifetime spectrometer (FLS) that was capable of simultaneous spectral and temporal resolution (Pitts and Mycek 2001). These experimental results were then compared with predictions from computational simulations. Descriptions of the instrumentation, phantom preparation and data processing are outlined below.

3.1. Instrumentation

A schematic of the modified FLS used for this study is depicted in figure 2 (Pitts and Mycek 2001). Briefly, a pulsed nitrogen laser (VSL-337, Laser Science Inc., Franklin, MA) was used as an excitation source at 337.1 nm, with a pulse width of 4 ns. This excitation light was coupled into a quartz fibre optic (600 μm diameter, 0.22 NA, SFS600/660N, Fiberguide Industries,

Table 1. Range of scattering coefficients for phantoms denoted media 1–5. Also shown are the measured and simulated apparent fluorescence lifetimes for these phantoms in the single-fibre geometry ($\rho = 0$, with standard deviations in parentheses). All listed values are at 550 nm.

Phantom	μ_s (cm^{-1})	Experimental lifetime τ_e (ns)	Simulated lifetime τ_s (ns)
Medium 1	–	4.0 (0.1)	4.00 (0.02)
Medium 2	258 (25)	4.0 (0.1)	4.02 (0.02)
Medium 3	413 (25)	4.0 (0.1)	4.02 (0.02)
Medium 4	516 (25)	3.8 (0.1)	4.03 (0.02)
Medium 5	590 (25)	4.0 (0.1)	4.04 (0.02)

Stirling, NJ) using a retractable mirror (RM, 5100, New Focus, Santa Clara, CA) and a quartz lens (L_1). This fibre was used to deliver light to the sample and would correspond to the source fibre in figure 1. Another identical fibre optic was used to collect the fluorescence emission from the sample (detector fibre in figure 1), which was then collimated through another lens (L_2). The light collected by the detector fibre was filtered for any residual excitation light by the dichroic mirror (DC) and an additional long pass filter (LP) after collimation and before reaching the beam splitter (BS).

For the temporally resolved measurement, the BS directed a portion of the beam to a high-speed avalanche photodiode module (APD) (C5658, Hamamatsu, Bridgewater, NJ) via a band-pass filter (BP) that could be used to control the spectral range of the emission reaching the APD. For the experiments reported here, the BP was centred at 550 $\pm$ 10 nm. The transient APD response was then digitized on a 1 GHz oscilloscope (TDS-680C, Tektronix, Willsonville, OR). For spectrally resolved measurements, the other portion of the split beam was coupled into another fibre for delivery into the entrance slit of a spectrograph (MS125, Oriel Instruments, Stratford, CT) equipped with a gated, intensified charged coupled device (ICCD, Andor Technology, Belfast, Northern Ireland) at the exit port. Removing the RM from the set-up allowed sample illumination and light collection using a single fibre optic (figure 2, dotted lines, or figure 1, $\rho = 0$).

3.2. Phantom preparation

Two sets of tissue phantoms were prepared by mixing solutions of fluorescein in de-ionized (DI) water with suspensions of 1 μm diameter polystyrene spheres (CAT 07310, PolySciences, MA). A phantom's absorption coefficient was dominated by fluorescein and was calculated by measuring the transmittance of a fluorescein solution in an absorption spectrophotometer (Cary Model #50; Varian Inc., Walnut Creek, CA) (Durkin *et al* 1993). The first set of phantoms prepared (media 1–5, table 1) had absorption coefficients $\mu_a = 0.004$ cm^{-1} (for DI water at 337 nm), $\mu_{af} \sim 0.75$ cm^{-1} (for a fixed concentration of 7×10^{-5} M fluorescein in DI water at 337 nm), while the second set (media 6–8) had absorption coefficients $\mu_a = 0.004$ cm^{-1}(for DI water at 337 nm), $\mu_{af} \sim 0.11$ cm^{-1} (for a fixed concentration of $\sim 1 \times 10^{-5}$ M fluorescein in DI water at 337 nm). A normalized spectrum from a solution of fluorescein in DI water was used to determine the wavelength-dependent fluorescence quantum yield, Φ_{QY}, needed for the simulation.

The scattering coefficient of each phantom was controlled by varying the per cent volume of the suspension occupied by the polystyrene spheres in the medium (Sefkow *et al* 2001). The wavelength dependence of the scattering coefficients for phantoms in table 1 (media 1–5) was calculated from the Mie theory (Sefkow *et al* 2001) and these data are shown in figure 3.

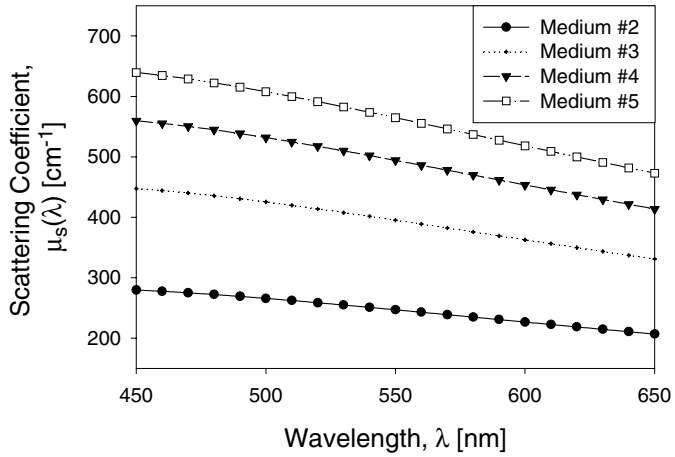

Figure 3. Scattering coefficients for the phantoms listed in table 1.

The second set of tissue phantoms had scattering coefficients $\mu_s = 400\ (\pm 25)\ \mathrm{cm}^{-1}$, $\mu_s = 290\ (\pm 25)\ \mathrm{cm}^{-1}$ and $\mu_s = 160\ (\pm 25)\ \mathrm{cm}^{-1}$, for medium 6, medium 7 and medium 8, respectively. These scattering coefficients are similar to the values reported for the optical scattering of biological tissues (Cheong *et al* 1990).

It was observed previously that polystyrene spheres can collisionally quench fluorescein fluorescence at fluorescein concentration $\sim 1 \times 10^{-5}$ M, as indicated by the linear decrease in fluorescein lifetime with increasing quencher (polystyrene sphere) concentration as per the Stern–Volmer equation (Vishwanath and Mycek 2002). The first set of phantoms (media 1–5, table 1) was prepared with a higher (fixed) concentration of fluorescein $\sim 7 \times 10^{-5}$ M, where collisional quenching was negligible (Vishwanath and Mycek 2002), as shown below. These phantoms were used for studies in the single-fibre geometry ($\rho = 0$). The second set of tissue phantoms (media 6 and 7) was prepared using a lower (fixed) concentration of fluorescein $\sim 1 \times 10^{-5}$ M for studies employing the dual-fibre geometry ($\rho \neq 0$). In this case, quenching effects were accounted for in the data analysis, as described below. It was determined experimentally that both concentrations of fluorescein used (a) were devoid of artefacts arising from reabsorption (inner filter) effects (Lakowicz 1999) and (b) generated fluorescence signal strengths comparable to those emanating from tissue *in vivo* (Pitts and Mycek 2001). To maintain matched boundary conditions between the optical fibres and the tissue phantom, both the source and detector fibres were placed with their tips well inside the turbid medium.

3.3. Data collection and analysis

Both spectrally and temporally resolved fluorescence data were collected for the set of phantoms indicated in table 1 by using the FLS in a single fibre geometry ($\rho = 0$) and for the second set of phantoms (media 6–8) by varying the source–detector distance ρ between 0 and 1 cm. Computational simulations, with appropriate tissue coefficients, were run to match these experiments, as described in section 4.

FLS data analysis was described in detail previously (Pitts and Mycek 2001). Briefly, the FLS was calibrated spectrally for both wavelength and absolute fluorescence intensity. Wavelength calibration was achieved using a mercury–argon lamp (Model 6035, Oriel

Instruments) with reference to known emission lines. Correction for the FLS spectral instrument response was achieved by dividing the measured spectra with a wavelength-dependent sensitivity factor, $S(\lambda)$ (Pitts and Mycek 2001). $S(\lambda)$ was calculated by measuring the irradiance, $M_{\mathrm{Lamp}}(\lambda)$, from a NIST-traceable tungsten halogen lamp (63355 SN 7-1329, Oriel Instruments) and dividing this spectrum by the known theoretical spectrum, $T_{\mathrm{Lamp}}(\lambda)$, provided by the manufacturer: $S(\lambda) = M_{\mathrm{Lamp}}(\lambda)/T_{\mathrm{Lamp}}(\lambda)$. All measurements and theoretical spectra were converted from units of energy to absolute photon numbers (quanta), creating a unitless $S(\lambda)$. By determining $S(\lambda)$ in this way, the collection of distortion-free emission intensity spectra measured in photon numbers was possible.

Measured fluorescence spectral data were corrected for background contributions by subtraction of a pre-recorded background spectrum and for non-uniformity of the instrument response by division with the wavelength-dependent sensitivity factor $S(\lambda)$. Thus, $M_{\mathrm{corr}}(\lambda) = (M(\lambda) - B(\lambda))/S(\lambda)$, where $M_{\mathrm{corr}}(\lambda)$ is the corrected spectrum, $M(\lambda)$ is the measured sample emission, and $B(\lambda)$ the background spectrum. $M(\lambda)$ and $B(\lambda)$ were measured in units of CCD counts per nanometre, a linear measure of photon numbers (quanta) arriving at the detector, and $S(\lambda)$ was unitless.

Measured time-resolved data, $M(t)$, contained the actual fluorescence signal, $F(t)$, along with an instrument response, $I(t)$. This instrument response function contained distortions due to the response of the electronics, the optics and the finite duration of the excitation pulse. To correct for these artefacts, the instrument response was measured as the fluorescence signal from a 1×10^{-6} M solution of Rose Bengal in DI water, which had a lifetime of $\sim$90 ps (Kolber and Barkley 1986) (well below the temporal resolution of the FLS (Pitts and Mycek 2001)). Thus, the measured fluorescence signal from a phantom $M(t)$ was interpreted as the convolution of the instrument response, $I(t)$, with the actual fluorescence signal, $F(t)$. Measured fluorescence decays were analysed using a least-squares iterative reconvolution procedure based on the Marquardt algorithm (Light Analysis, Quantum Northwest, Inc., WA), to extract the best-fit lifetime (Pitts and Mycek 2001). For phantom experiments with fluorescein $F(t)$ was best fit to a single exponential decay, $F(t) \sim \exp(-t/\tau)$, where τ is the phantom's observed lifetime. As shown below, the value of τ extracted using this fitting method was not necessarily equal to the intrinsic fluorophore lifetime due to perturbations on the intrinsic time-resolved fluorescence decay caused by propagation in the presence of optical scattering in the phantom.

4. Computational results and discussion

For each simulation run, the numerical aperture used for each fibre was infinite (the simulation detected every photon that lay within the fibre area irrespective of the exit angle of the photon), and the fibre diameter used was 0.1 cm.

4.1. Validation with diffusion theory and prior studies

The Monte Carlo model described above was programmed and its performance was validated against diffusion theory and prior studies (Wang *et al* 1995), for spatial and time-resolved reflectance and fluorescence expressions from a semi-infinite medium with matched boundary conditions. Figure 4 shows comparisons of the simulation used in this study (filled circles), diffusion theory (equation (4), solid line), and a previously published model (Wang *et al* 1995) (hollow circles) for the prediction of normalized diffuse reflectance versus source–detector separation for a turbid, homogeneous, semi-infinite medium with optical coefficient: $\mu_a = 0.05\ \mathrm{cm}^{-1}$, $\mu_s = 5\ \mathrm{cm}^{-1}$ and $g = 0.73$. The simulation's predicted decrease of reflectance

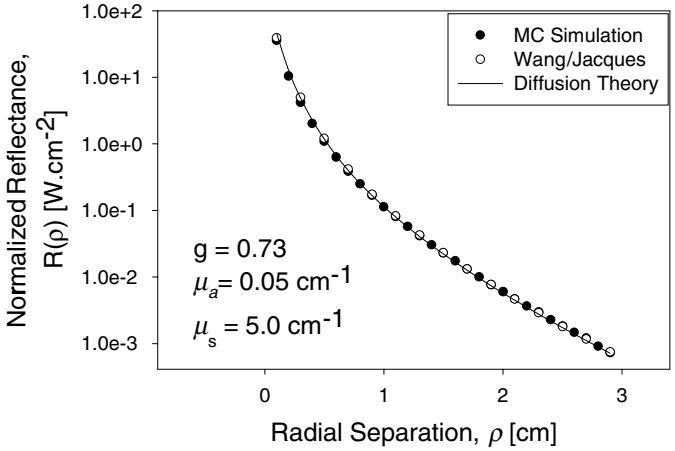

Figure 4. Comparisons of the simulation used in this study (filled circles), diffusion theory (equation (4), solid line), and a previously published model (Wang *et al* 1995) (hollow circles) for the prediction of normalized diffuse reflectance versus source–detector separation for a turbid, homogeneous, semi-infinite medium with optical properties as shown.

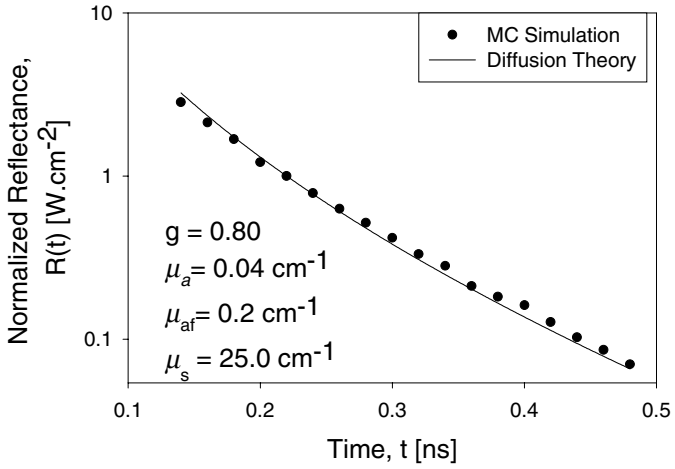

Figure 5. Comparison of simulation (filled circles) with diffusion theory (equation (10), solid line) for time-resolved reflectance from a homogeneous, turbid, semi-infinite medium with optical coefficients as shown. The simulation results were obtained for single-fibre geometry.

with increasing ρ agrees quantitatively with theory and prior results to better than 4%. Figure 5 shows a comparison of our simulation (filled circles) with diffusion theory (equation (10), solid line) for time-resolved reflectance from a homogeneous, turbid, semi-infinite medium with optical coefficients: $\mu_a = 0.04\,\mathrm{cm}^{-1}$, $\mu_{af} = 0.2\,\mathrm{cm}^{-1}$, $\mu_s = 50\,\mathrm{cm}^{-1}$ and $g = 0.8$. The simulation results were obtained for single-fibre geometry ($\rho = 0$). The simulation's predicted decrease in reflectance with increasing time agrees with the diffusion theory to within 8%. Thus, for both steady-state and time-resolved reflectance cases, the simulation provided good agreement with theory and prior studies over the parameter space appropriate for diffusive photon propagation in turbid media.

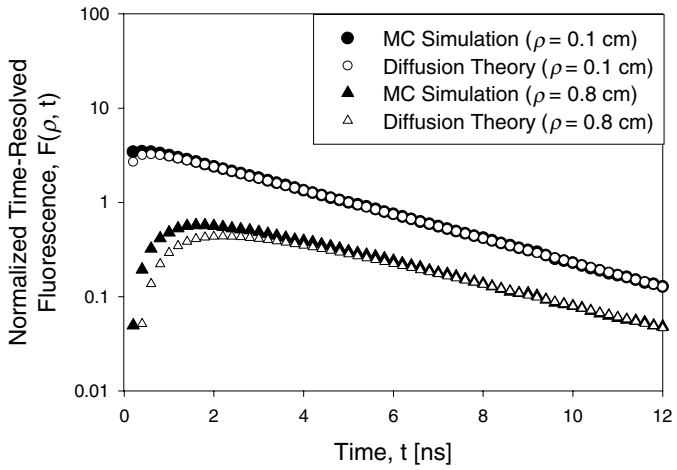

Figure 6. Comparison of simulation (filled symbols) with diffusion theory (equation (10), hollow symbols) for time-resolved fluorescence emanating from a homogeneous, turbid, semi-infinite medium with a concentration of a single fluorophore species of lifetime $\tau = 3.4$ ns and optical coefficients ${}^{x}\mu_a = {}^{m}\mu_a = 0.004$ cm^{-1}, ${}^{x}\mu_s = {}^{m}\mu_s = 290$ cm^{-1}, $\mu_{af} = 0.25$ cm^{-1} and ${}^{x}g = {}^{m}g = 0.8$. The circles indicate a source–detector separation $\rho = 0.1$ cm. The triangles indicate a source–detector separation $\rho = 0.8$ cm.

Figure 6 shows the time-resolved fluorescence from a semi-infinite medium containing a single fluorophore species (of lifetime $\tau_F = 3.4$ ns) as modelled by the simulation (filled triangles and filled circles), along with predictions from diffusion theory (equation (12), hollow triangles and hollow circles). The theoretical prediction for time-resolved fluorescence emanating from a fluorophore with a finite lifetime was obtained by performing the indicated convolution in equation (12) numerically. The semi-infinite medium's optical properties were: ${}^{x}\mu_a = {}^{m}\mu_a = 0.004$ cm^{-1}, ${}^{x}\mu_s = {}^{m}\mu_s = 290$ cm^{-1}, $\mu_{af} = 0.2$ cm^{-1}, and ${}^{x}g = {}^{m}g = 0.8$. The curves indicated by the circles represent the time-resolved fluorescence with source–detector separation $\rho = 0.1$ cm, while the curves marked by the triangles were for $\rho = 0.8$ cm.

Figure 6 shows that the overall intensity of the detected fluorescence emission decreased by approximately one order of magnitude at large source–detector separations due to photon losses from the $\exp(-\rho^2)$ term of equation (12), as expected. In the figure, each simulation has been normalized to the corresponding theoretical prediction at time $t = 10$ ns to better reveal differences in the temporal decay characteristics between datasets. At a small source–detector separation ($\rho = 0.1$ cm), both the diffusion theory and the simulation (circles) revealed the expected single exponential decay of fluorescence emission in time. At a larger source–detector separation ($\rho = 0.8$ cm), however, the decay was more complicated with a delayed onset of nearly 2 ns, followed by the expected mono-exponential decay. We also note that it is apparent from figure 6 that the simulated and theoretical values are in good agreement for small source–detector separations, while there is a discrepancy in observed fluorescence decays for larger separations. The significance of the differing dynamics observed here and their impact on recovered fluorescence lifetimes in scattering media are investigated further by comparison to experiments in the dual-fibre geometry ($\rho \neq 0$) as described in section 4.3.

4.2. Comparison with experiment: single-fibre geometry

The series of phantom media listed in table 1 were prepared as described in section 3 for fluorescence measurements using the FLS in the single-fibre configuration ($\rho = 0$). Figure 7(a)

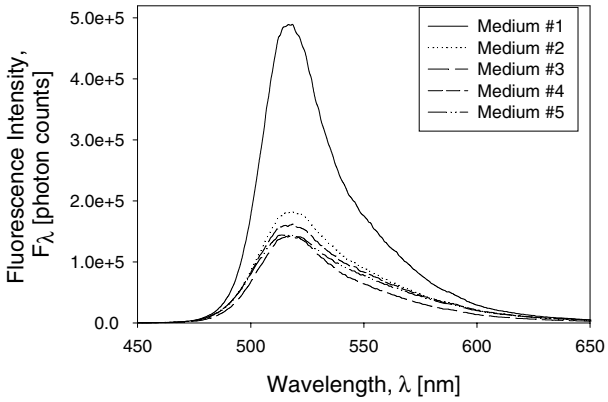

(a)

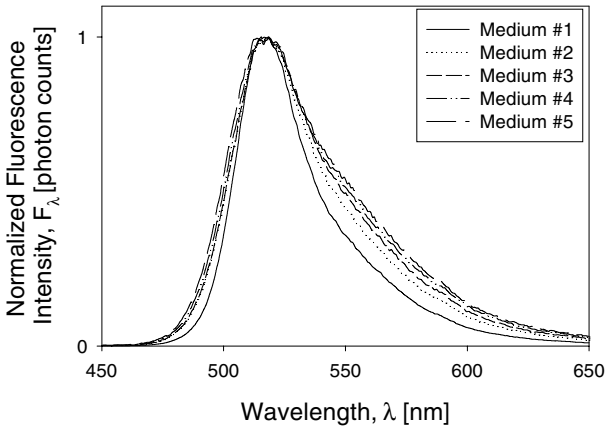

(b)

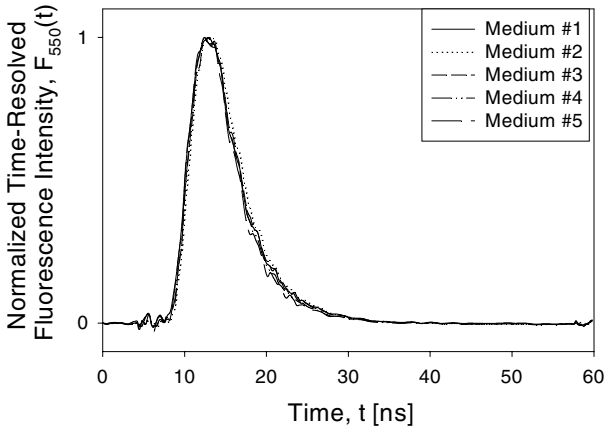

(c)

Figure 7. (a) Measured steady-state fluorescence spectra collected from the phantom media indicated in table 1 using a single-fibre geometry ($\rho = 0$). Medium 1 was a solution of fluorescein in DI water with no scattering present. (b) Normalized spectra from (a), showing increasing spectral distortions introduced with increasing scattering. (c) Normalized time-resolved fluorescence decays corresponding to spectra in (a) and (b) showed no distortions due to increased scattering.

shows the measured steady-state fluorescence spectra, which decreased sharply in intensity with increasing scattering, as expected. When the peak intensity of each spectrum in figure 7(a) was normalized to unity (figure 7(b)), it became apparent that spectral artefacts had manifested in the data obtained from the scattering phantoms (media 2–5). The dominant artefact was an increased redshift in the spectrum with increased scattering. This apparent redshift resulted from the relative increase in blue–green scattering (see $\mu_s(\lambda)$, figure 3) and hence decrease in detected blue–green emission for scattering phantoms (media 2–5) versus the phantom with no scattering present (medium 1). While scattering-induced artefacts were observed in the fluorescence spectra, the corresponding time-resolved fluorescence decays showed no apparent distortions (figure 7(c)). These transient decays were analysed to extract lifetime values, as listed in table 1 under the column labelled experimental lifetimes. Also presented in table 1 are lifetimes obtained from Monte Carlo simulations run with optical properties corresponding to each phantom (media 1–5). The lifetime of 7×10^{-5} M fluorescein, in solution with DI-water (pH $\sim$ 7) with no scattering suspension added (medium 1), as measured by the FLS ($\tau_F = 4.0$ ns) was used for input into the simulation as the real lifetime of fluorescein. For both experiment and simulation, lifetime values obtained for all media in the single-fibre geometry were unchanged by the presence of scattering, as indicated in table 1 (we note that this verifies that collisional quenching was negligible in this phantom set). This observation reflects the general fact that intrinsic fluorophore lifetimes remain unaffected by variations in excitation intensity or sources of optical loss (Lakowicz 1999), in this case due to the presence of scattering in turbid media. This feature of fluorophore lifetime spectroscopy, referred to as intensity independence, is considered an advantage over intensity-dependent steady-state spectral measurements. In the next section, we will explore the potential limitations to this feature, which should be considered when working in turbid media with multiple optical fibres.

4.3. Comparison with experiment: dual-fibre geometry

To further investigate the effects of scattering on observed fluorophore lifetimes with varying source–detector separation, the FLS was used in its dual-fibre configuration, as indicated schematically in figures 1 and 2, to perform time-resolved measurements on biological tissue phantoms (media 6–8). As observed for the single-fibre geometry (figures 7(a) and (b)), steady-state fluorescence spectra collected for each phantom when the centres of source and detector fibres were separated from each other by a distance of twice the fibre radius (the minimum separation achievable experimentally) revealed increasing spectral distortions with increasing scattering (data not shown). Time-resolved fluorescence decays were collected for each of media 6–8 for varying source–detector separations ($\rho = 0.1$ cm to 0.7 cm). In contrast with fluorescence lifetime measurements in the single-fibre geometry (figure 7(c)), increases in the observed lifetime (τ) were detected with increased scattering in the dual-fibre geometry.

We note that experimental fluorescence decays were analysed as described in section 3.3 in order to extract observed lifetimes τ for each medium, at each source–detector position. For these analyses, instrument response functions $I(t)$ were measured at each source–detector separation ρ and each resulting $I(\rho, t)$ was used for iterative-reconvolution fits to data. As $I(\rho, t)$ functions were measured in scattering free solutions, the calculated lifetime (at any particular source–detector separation) was invariant to which particular $I(\rho, t)$ was used in the iterative-reconvolution procedure. Therefore, for all the analyses presented here, the instrument response measured when the source–detector separation was the minimum achievable experimentally ($\sim$600 μm) was the one used in iterative-reconvolution fits of the measured experimental data. For theoretical decays, the apparent fluorophore lifetime was obtained from the slope of a straight-line fit to the negative natural logarithm of the convolved

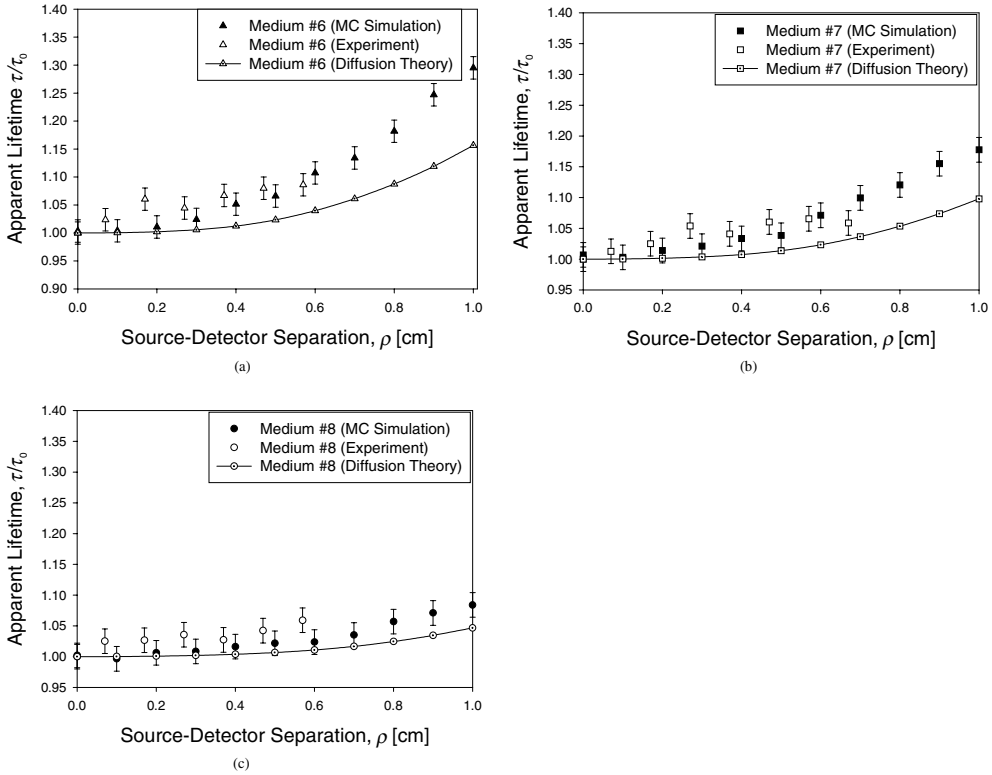

Figure 8. (a) Apparent lifetime increase with increasing source–detector separations as observed experimentally (hollow triangles) and as predicted by simulation (filled triangles) and diffusion theory (dotted triangles with solid line). The medium's scattering coefficient was 400 cm^{-1} at 550 nm. (b) Apparent lifetime increase with increasing source–detector separations as observed experimentally (hollow squares) and as predicted by simulation (filled squares) and diffusion theory (dotted squares with solid line). The medium's scattering coefficient was 290 cm^{-1} at 550 nm. (c) Apparent lifetime increase with increasing source–detector separations as observed experimentally (hollow circles) and as predicted by simulation (filled circles) and diffusion theory (dotted circles with solid line). The medium's scattering coefficient was 160 cm^{-1} at 550 nm.

theoretical fluorescence expression (equation (12)) in time. The single-exponential fit was performed after a lapse of 4 ns with respect to the δ-function excitation source and was optimized using a least-squares analysis. An analogous procedure was employed to obtain the apparent lifetime from the simulated time-resolved fluorescence signals. Each point for a predicted simulation lifetime value was the average of four identical simulation runs, where each run launched 1×10^7 photons. Varying the lapse time between 3 ns and 6 ns changed the recovered lifetimes from either the analytical expression or the simulation by less than $\sim$3%. These methods enabled us to analyse and compare time-resolved fluorescence decays from experiment, theory and simulation for significant propagation delays caused by optical scattering.

Figures 8(a), (b) and (c) show the increase in apparent fluorophore lifetime with increasing source–detector separations (ρ) for medium 6, medium 7 and medium 8, respectively. At 550 nm, the scattering coefficient of medium 6 was 400 cm^{-1}, that of medium 7 was 290 cm^{-1}, and that of medium 8 was 160 cm^{-1}. In each figure, the solid, hollow and dotted (with a solid line) symbols represent data as modelled by simulations, measured

experimentally, and predicted by diffusion theory, respectively. In order to quantitatively compare experimental, computational and theoretical results across phantom media with differing scattering properties, a normalization procedure was employed. Thus, for all data in figures 8, the observed lifetime τ at each source–detector position ρ was divided by a normalization lifetime, τ_0. For the curves representing theoretical and simulated predictions, the normalization lifetime used was the real lifetime of the fluorophore (which was used both in equation (12) and as input to the simulation). The value the normalization lifetime τ_0 used in simulation and calculations was 3.4 ns (lifetime of 1×10^{-5} M fluorescein in DI water (Yianzeng 2000)). For the experimental data, the normalization lifetime τ_0 for each phantom was taken to be the lifetime of the fluorophore measured in that medium using the FLS in a single-fibre configuration ($\rho = 0$). This procedure effectively eliminated effects due to variations in lifetime resulting from collisional quenching of fluorescein by the polystyrene spheres (Lakowicz 1999, Vishwanath and Mycek 2002) and allowed quantitative comparisons of apparent lifetime increases as determined by experiment, simulation and theory for each phantom medium used.

Figure 8 shows that all phantoms (media 6–8) revealed an increase in apparent fluorophore lifetime (τ/τ_0) with increasing source–detector separation (ρ). This increase in apparent lifetime was greatest for medium 6, which had the highest scattering ($\mu_s = 400$ cm^{-1}, figure 8(a)), reaching predicted deviations of approximately 30% for $\rho = 1.0$ cm. Even at the lowest scattering ($\mu_s = 160$ cm^{-1}, medium 8, figure 8(c)), deviations at $\rho = 1.0$ cm were $\sim$9%. These relatively large increases in apparent lifetime were detected only in the dual-fibre geometry for source–detector separations larger than $\sim$0.5 cm and are attributed to the accumulated propagation delays induced by optical scattering, as illustrated by the time-resolved plots in figure 6.

In each of figures 8(a)–(c), diffusion theory predictions of apparent lifetimes underestimated the increases predicted by the simulations, while the simulations approximated the experimentally observed values. For instance, at $\rho \sim 0.4$ cm, for medium 6, diffusion theory calculations predicted a less than 4% increase in apparent lifetime, while simulations estimated the apparent increase to be $\sim$10%, as was observed by experimental measurements (figure 8(a)). At $\rho = 1.0$ cm, diffusion theory predicted at most a 15% increase in observed lifetime (at the highest scattering, figure 8(a)), while simulations predicted an increase of nearly 30%. This value of $\rho = 1.0$ cm was chosen in order to represent an upper limit for typical clinical fibre-probe designs. For all phantoms, experimental values closely followed simulations until signal loss at high source–detector separations ($\rho > 0.6$ cm) precluded experimental detection.

The results discussed here, in combination with the data in figure 6, indicate that the lineshapes of the simulated time-resolved fluorescence decays increasingly differ in comparison with equation (12) (diffusion theory) with increasing source–detector separation. Recent studies have suggested that the expression for time-resolved reflectance obtained from the diffusion approximation (equation (10)) may have to be modified to treat diffusive photon propagation in turbid media as having evolved from ballistic propagation at earlier times (Cai *et al* 2000, 2002, Xu *et al* 2001). It is possible that the theoretical results presented in this study could be improved by employing such modified analytical expressions to describe time-resolved reflectance (fluorescence) from turbid media. Studies incorporating these improved theoretical approximations to model time-resolved fluorescence are under investigation.

In summary, increased polystyrene sphere concentration or increased source–detector separation increased the apparent lifetime recovered experimentally, predicted theoretically or simulated numerically. For the range of scattering values studied here, this effect was

negligible for the single-fibre probe geometry and for source–detector separations $\rho < 0.2$ cm. We note that using quantitative predictions from a simulation such as the one presented here, it may be possible to correct for scattering-induced effects on observed fluorophore lifetimes if both the medium's optical properties and the source–detector geometry are known. Further extensions of the model to simulate multi-layered media are under development.

5. Conclusions

To quantify the effects of optical scattering on fluorescence lifetimes recovered from biological systems, a Monte Carlo model capable of simulating time-resolved fluorescence propagation in a semi-infinite turbid medium was developed and validated against previously reported theoretical and computational models. The Monte Carlo simulation was then compared to experimental measurements on tissue-simulating phantoms with controlled absorption and scattering properties. Although fluorescence lifetime measurements are generally more robust to scattering artefacts than are measurements of fluorescence spectra (as observed here in studies using a single fibre-optic probe for illumination and detection), scattering induced changes in apparent fluorophore lifetime as large as 30% were found when spatially separated source and detector fibres were used. Quantitative simulations such as those presented here should aid in the accurate recovery of fluorescence lifetimes from turbid biological systems.

Acknowledgments

This work was supported by the American Cancer Society Institutional Research grant no IRG-82-003-17 (M-AM), the National Science Foundation grant no BES-9977992 (M-AM), The Whitaker Foundation (M-AM) and the National Cancer Institute grants RO1CA78734 (BWP) and PO1CA80139 (BWP).

References

Alfano R R *et al* 1998 *Advances in Optical Biopsy and Optical Mammography* vol 838, ed R R Alfano (New York: The New York Academy of Sciences) pp 14–28

Beauvoit B and Chance B 1998 Time-resolved spectroscopy of mitochondria, cells and tissues under normal and pathological conditions *Mol. Cell. Biochem.* **184** 445–55

Cai W, Lax M and Alfano R R 2000 Cumulant solution of the elastic Boltzmann transport equation in an infinite uniform medium *Phys. Rev. E Stat. Phys. Plasmas Fluids Relat. Interdiscip. Topics* **61** 3871–6

Cai W, Xu M, Lax M and Alfano R R 2002 Diffusion coefficient depends on time, not on absorption *Opt. Lett.* **27** 731–3

Cashwell E D and Everett C J 1959 *A Practical Manual on the Monte Carlo Method for Random Walk Problems* (New York: Pergamon)

Chandrasekhar S 1960 *Radiative Transfer* (New York: Dover)

Cheong W-F, Prahl S and Welch S 1990 A review of the optical properties of biological tissues *IEEE J. Quantum Electron.* **26** 2166–85

Das B B, Feng L and Alfano R R 1997 Time-resolved fluorescence and photon migration studies in biomedical and model random media *Rep. Prog. Phys.* **60** 227–92

Dhingra J, Perreault D J, McMillan K, Rebeiz E, Kabani S, Manohran R, Itzkan I, Feld M and Shapshay S 1996 Early diagnosis of upper aerodigestive tract cancer by autofluorescence *Arch. Otolaryngol. Head Neck Surg.* **122** 1181–6

Durkin A J, Jaikumar S and Richards-Kortum R 1993 Optically dilute, absorbing, and turbid phantoms for fluorescence spectroscopy of homogeneous and inhomogeneous samples *Appl. Spectrosc.* **47** 2114–21

Fantini S, Franceschini M A, Fishkin J B, Barbieri B and Gratton E 1994 Quantitative determination of the absorption spectra of chromophores in strongly scattering media: a light-emitting-diode based technique *Appl. Opt.* **33** 5204–13

Farrell T J, Patterson M S and Wilson B C 1992 A diffusion theory model of spatially resolved, steady-state diffuse reflectance for the noninvasive determination of the tissue optical properties *in vivo Med. Phys.* **19** 879–88

Flock S, Wilson B and Patterson M 1989 Monte Carlo modeling of light propagation in highly scattering tissues: II. Comparsion with measurements in phantoms *IEEE Trans. Biomed. Eng.* **36** 1169–73

Frisoli J K, Tudor E G, Flotte T J, Hassan T, Deutsch T F and Schomacker K T 1993 Pharmokinetics of fluorescent drug using laser-induced fluorescence *Cancer Res.* **53** 5954–61

Glanzmann T 1998 *Thesis* Institute of Environmental Engineering, Swiss Federal Institute of Technology of Lausanne, Lausanne, Switzerland (submitted)

Haskell R C 1994 Boundary conditions for the diffusion equation in radiative transfer *J. Opt. Soc. Am.* A **11** 2727–41

Hattery D, Chernomordik V, Loew M, Gannot I and Gandjbakhche A 2001 Analytical solutions for time-resolved fluorescence lifetime imaging in a turbid medium such as tissue *J. Opt. Soc. Am.* A **18** 1523–30

Henyey L G and Greenstein J L 1941 Diffuse radiation in the galaxy *Astrophys. J.* **93** 70–83

Hutchinson C L, Lakowicz J R and Sevick-Muraca E M 1995 Fluorescence lifetime-based sensing in tissue: a computational study *Biophys. J.* **68** 1574–82

Hutchinson C L, Troy T L and SevickMuraca E M 1996 Fluorescence-lifetime determination in tissues or other scattering media from measurement of excitation and emission kinetics *Appl. Opt.* **35** 2325–32

Jacques S L 1989 Time resolved propagation of ultrashort laser pulses within turbid tissue *Appl. Opt.* **28** 2223–9

Kienle A and Patterson M S 1997 Improved solutions of the steady-state and the time-resolved diffusion equations for reflectance from a semi-infinite turbid medium *J. Opt. Soc. Am.* A **14** 246–54

Kolber Z S and Barkley M D 1986 Comparison of approaches to the instrument response function in fluorescence decay measurements *Anal. Biochem.* **152** 6–21

Konig K, Ruck A and Schneckenburger H 1992 Fluorescence detection and photodynamic activity of endogenous protoporphyrin in human skin *Opt. Eng.* **31** 1470–4

Lakowicz J R 1999 *Principles of Fluorescence Spectroscopy* (New York: Kluwer)

Lee K C B, Siegel J, Webb S E D, Leveque-Fort S, Cole M J, Jones R, Dowling K, Lever M J and French P M W 2001 Application of the stretched exponential function to fluorescence lifetime imaging *Biophys. J.* **81** 1265–74

Lux I and Koblinger L 1991 *Monte Carlo Particle Transport Methods: Neutron and Photon Calculations* (Boca Raton, FL: CRC Press)

Mourant J, Boyer J, Hielscher A H and Bigio I J 1996 Influence of the scattering phase function on light transport measurements in turbid media performed with small source–detector separations *Opt. Lett.* **21** 546–8

Mycek M-A, Schomacker K and Nishioka N 1998 Colonic polyp differentiation using time resolved autofluorescence spectroscopy *Gastrointest. Endosc.* **48** 390–4

Mycek M-A, Vishwanath K, Schomacker K T and Nishioka N S 2000 *Biomedical Topical Meetings* (Optical Society of America Technical Digest) pp 11–3

Paithankar D Y, Chen A U, Pogue B W, Patterson M S and Sevick-Muraca E M 1997 Imaging of fluorescent yield and lifetime from multiply scattered light reemitted from random media *Appl. Opt.* **36** 2260–72

Paithankar D Y, Schomacker K T and Nishioka N S 1999 Frequency-domain optical detection of subsurface blood vessels: Experimental and computational studies using a scattering phantom *IEEE J. Sel. Top. Quantum Electron.* **5** 1032–9

Patterson M, Chance B and Wilson B 1989 Time resolved reflectance and transmittance for the non-invasive measurement of tissue optical properties *Appl. Opt.* **28** 2331–6

Patterson M S and Pogue B W 1994 Mathematical model for time-resolved and frequency-domain fluorescence spectroscopy in biological tissues *Appl. Opt.* **33** 1963–74

Pfeifer L, Schmalzigaug K, Paul R, Lichey J, Kemnitz K and Fink F 1995 Time-resolved autofluorescence measurements for the differentiation of lung-tissue states *Proc. SPIE* **2627** 129–35

Pitts J D and Mycek M-A 2001 Design and development of a rapid acquisition laser-based fluorometer with simultaneous spectral and temporal resolution *Rev. Sci. Instrum.* **72** 3061–72

Pogue B W and Burke G 1998 Fiber-optic bundle design for quantitative fluorescence measurement from tissue *Appl. Opt.* **37** 7429–36

Pogue B W, Pitts J D, Mycek M-A, Sloboda R D, Wilmot C, Brandsema J A and O'Hara J A 2001 *In vivo* NADH fluorescence monitoring as an assay for cellular damage in photodynamic therapy *Photochem. Photobiol.* **74** 817–24

Pradhan A, Das B B, Yoo K M, Cleary J, Prudente R, Celmer E and Alfano R R 1992 Time-resolved UV photoexcited fluorescence kinetics from malignant and non-malignant human breast tissue *Lasers Life Sci.* **4** 225–34

Prahl S A 1988 *Thesis* University of Texas at Austin, TX

Richards-Kortum R 1995 *Optical-Thermal Response of Laser Irradiated Tissue* ed A J Welch and M J C van Gemert (New York: Plenum) pp 667–707

Richards-Kortum R and Sevick-Muraca E 1996 Quantitative optical spectroscopy for tissue diagnosis *Annu. Rev. Phys. Chem.* **47** 555–606

Rudolph W and Kempe M 1997 Topical review: trends in optical biomedical imaging *J. Mod. Opt.* **44** 1617–42

Sadoqi M, Riseborough P and Kumar S 2001 Analytical models for time resolved fluorescence spectroscopy in tissues *Phys. Med. Biol.* **46** 2725–43

Schomacker K T, Frisoli J K, Compton C C, Flotte T J, Richter J M and Deutsch T F 1992 Ultraviolet laser-induced fluorescence of colonic polyps *Gastroenterology* **102** 1155–60

Sefkow A, Bree M and Mycek M-A 2001 A method for measuring cellular optical absorption and scattering evaluated using dilute cell suspension phantoms *Appl. Spectrosc.* **55** 1495–501

Sevick-Muraca E M, Reynolds J S, Troy T L, Lopez G and Paithankar D Y 1998 *Advances in Optical Biopsy and Optical Mammography* ed R R Alfano (New York: The New York Academy of Sciences) pp 46–57

Song Z, Dong K, Hu X H and Lu J Q 1999 Monte Carlo simulation of converging laser beams propagating in biological materials *Appl. Opt.* **38** 2944–9

Star W M, Marijnissen J P A and van-Gemert M J C 1988 Light dosimetry in optical phantoms in tissues: I. Multiple flux and transport theory *Phys. Med. Biol.* **33** 437–54

Testorf M, Osterberg U, Pogue B and Paulsen K 1999 Sampling of time- and frequency-domain signals of Monte Carlo simulations of photon migration *Appl. Opt.* **38** 236–45

Vaupel P, Kallinowski F and Okunieff P 1989 Blood flow, oxygen and nutrient supply, and metabolic microenvironment of human tumors: a review *Cancer Res.* **49** 6449–65

Vishwanath K and Mycek M-A 2002 Polystyrene microspheres in tissue-simulating phantoms can collisionally quench fluorescence *J. Fluoresc.* (to be published)

Wagnières G, Star W and Wilson B 1998 *In vivo fluorescence spectroscopy and imaging for oncological applications Photochem. Photobiol.* **68** 603–32

Wang L, Jacques S L and Zheng L 1995 MCML—Monte Carlo modeling of photon transport in multi-layered tissues *Comput. Methods Programs Biomed.* **47** 131–46

Wang L V, Nordquist R E and Chen W R 1997 Optimal beam size for light delivery to absorption-enhanced tumors buried in biological tissues and effect of multiple-beam delivery: a Monte Carlo study *Appl. Opt.* **36** 8286–91

Welch A J, Gardner C, Richards-Kortum R, Chan E, Criswell G, Pfefer J and Warren S 1997 Propagation of fluorescence light *Lasers Surg. Med.* **21** 166–78

Welch A J and van-Gemert M J C 1995 *Optical-Thermal Response of Laser-Irradiated Tissue* (New York: Plenum)

Wilson B C and Adam G 1983 A Monte-Carlo model for the absorption and flux distribution of light in tissue *Med. Phys.* **10** 824–30

Wu J, Feld M and Rava R 1993 Analytical model for extracting intrinsic fluorescence in turbid media *Appl. Opt.* **32** 3585–95

Xu M, Cai W, Lax M and Alfano R R 2001 Photon-transport forward model for imaging in turbid media *Opt. Lett.* **26** 1066–8

Yaroslavsky I V, Yaroslavsky A N, Tuchin V V and Schwarzmaier H J 1997 Effect of the scattering delay on time-dependent photon migration in turbid media *Appl. Opt.* **36** 6529–38

Yianzeng S 2000 Determination of fluorescence lifetime of sodium fluorescein *Chin. J. Anal. Chem.* **28** 1416–8

Zeng H, MacAulay C, McLean D I and Palcic B 1997 Reconstruction of *in vivo* skin autofluorescence spectrum from microscopic properties by Monte Carlo simulation *J. Photochem. Photobiol.* B **38** 234–40

Zeng H, Weiss A, Cline R and MacAulay C 1998 Real-time endoscopic fluorescence imaging for early cancer detection in the gastrointestinal tract *Bioimaging* **6** 151–65